The Determination of α_S and the Gluon Distribution in the Proton from HERA Data

M.R. Sutton
On behalf of the ZEUS and H1 Collaborations

University of Oxford, Dept. of Particle Physics,
Denys Wilkinson Building, Keble Road, Oxford OX1 3RH, Great Britain

Abstract

Recent precision measurements from the H1 and ZEUS collaborations of the inclusive cross-section and jet production in Neutral Current Deep Inelastic scattering at HERA are presented. Phenomenological fits to this data to determine the QCD coupling constant, α_S, and the gluon distribution within the proton performed by ZEUS and H1 are described. The description of the data by available next-to-leading order QCD calculations over many orders of magnitude is a major triumph of perturbative QCD. The precision of the steeply rising gluon density is better than 10% at lower x and that of the complementary measurements of α_S approach the world average with the dominant uncertainty now arising from theoretical sources.

1 Introduction

The Deep Inelastic Scattering (DIS) of a lepton probe from a target proton provides an important environment for the study of perturbative QCD and the structure of the proton. The HERA collider is unique in that it collides a lepton beam with a proton beam with a centre of mass energy of 318GeV and before 1998, 300GeV, higher than at any other facility and equivalent to a fixed target lepton-beam energy of over 50TeV. This allows the extension of the kinematic plane in DIS by several orders of magnitude in both the photon virtuality, Q^2, and x, the fraction of the proton momentum carried by the struck parton.

The rapid rise of the proton structure function, F_2 towards low x first observed at HERA [1], is attributed to a large gluon density within the proton. With the new, high precision data now becoming available from the colliding beam experiments, ZEUS and H1, HERA provides an excellent laboratory for the study of proton structure and the behaviour of QCD evolution over a very large kinematic region spanning five orders of magnitude in x and Q^2. A detailed understanding of the structure of the proton will be required in order to maximise the potential for the discovery of new physics at current and future colliders.

Recently, both ZEUS and H1 have completed new, high precision measurements of the inclusive neutral current (NC) cross-section [2] and jet production [3] in DIS using the e^+p data samples collected during the 1996-1997 running period. Using these data, both collaborations have performed next-to-leading order (NLO) fits to determine the parton distribution functions (PDF's) within the proton, and to determine the QCD coupling α_S, which is of fundamental importance to our understanding of perturbative QCD (pQCD). In this paper the determination of α_S and the gluon density in the proton using this new data will be described.

1.1 Inclusive DIS

The NC DIS cross-section for scattering of a positron from a proton target can be written as

$$\frac{\mathrm{d}^2\sigma^{\mathrm{NC}}(e^+p)}{\mathrm{d}x\mathrm{d}Q^2} = \frac{4\pi\alpha^2}{xQ^4}\left[(1-y+y^2/2)F_2(x,Q^2) - y(1-y/2)xF_3(x,Q^2) - \frac{y^2}{2}F_L(x,Q^2)\right], \tag{1}$$

where α is the electromagnetic fine structure constant, y the inelasticity parameter and Q^2 the virtuality of the exchanged boson. The F_3 structure function is related to the parity violating exchange of the Z^0 boson, and so is only significant for $Q^2 \gtrsim M_Z^2$. Because of the y^2 term, the longitudinal structure function, F_L, only contributes significantly at large y and the NC cross-section at low Q^2 and y is dominated by F_2.

Since the exchanged boson can only couple to quarks, to zeroth order, the scattering is only sensitive to the quark densities within the proton, with F_2 being given at low Q^2 by

$$F_2 = x\sum_i e_i^2(q_i(x) + \bar{q}_i(x)) \tag{2}$$

with the sum running over all accessible quark flavours, i, with corresponding charge e_i. The gluon distribution is therefore only accessible through higher order corrections, and hence strongly correlated with the coupling α_S. In this case the cross-section can be factorised into a convolution of the short range interaction with the parton distribution functions (PDF's), with the form of the PDF's given by some non-perturbative, short distance input distributions which are evolved using perturbative evolution equations.

NLO QCD fits to F_2 at intermediate Q^2, generally use the DGLAP evolution equations [4] to predict the Q^2 dependence of the parton distributions, but must use experimental data to constrain the x dependence of the input distributions at some starting scale, Q_0.

When addressing details of the partonic structure of the proton the question of in which regime the DGLAP evolution formalism breaks down and other evolution formalisms [5] take over should be addressed. For a discussion of these issues see elswhere in these proceedings [6].

1.2 Jet production and the hadronic final state

The inclusive cross-section and F_2 integrates over the properties of the final state, which are themselves dependent on α_S and the details of the perturbative hard subprocess. Studies of the hadronic final state in DIS, such as jet production in DIS and event shapes in the current region of the Breit frame [7] in DIS therefore allow determination of α_S and the gluon distribution in a fashion complementary to that from inclusive DIS.

Generally, the inclusive single jet production cross-section in DIS has a smaller renormalisation scale uncertainty than intrinsically higher order processes, such as dijet production. However, dijet production is to lowest order already an $\mathcal{O}(\alpha_S)$ process and so sensitive to α_S and the gluon distribution directly although the cross-section is correspondingly smaller and scale uncertainties more significant.

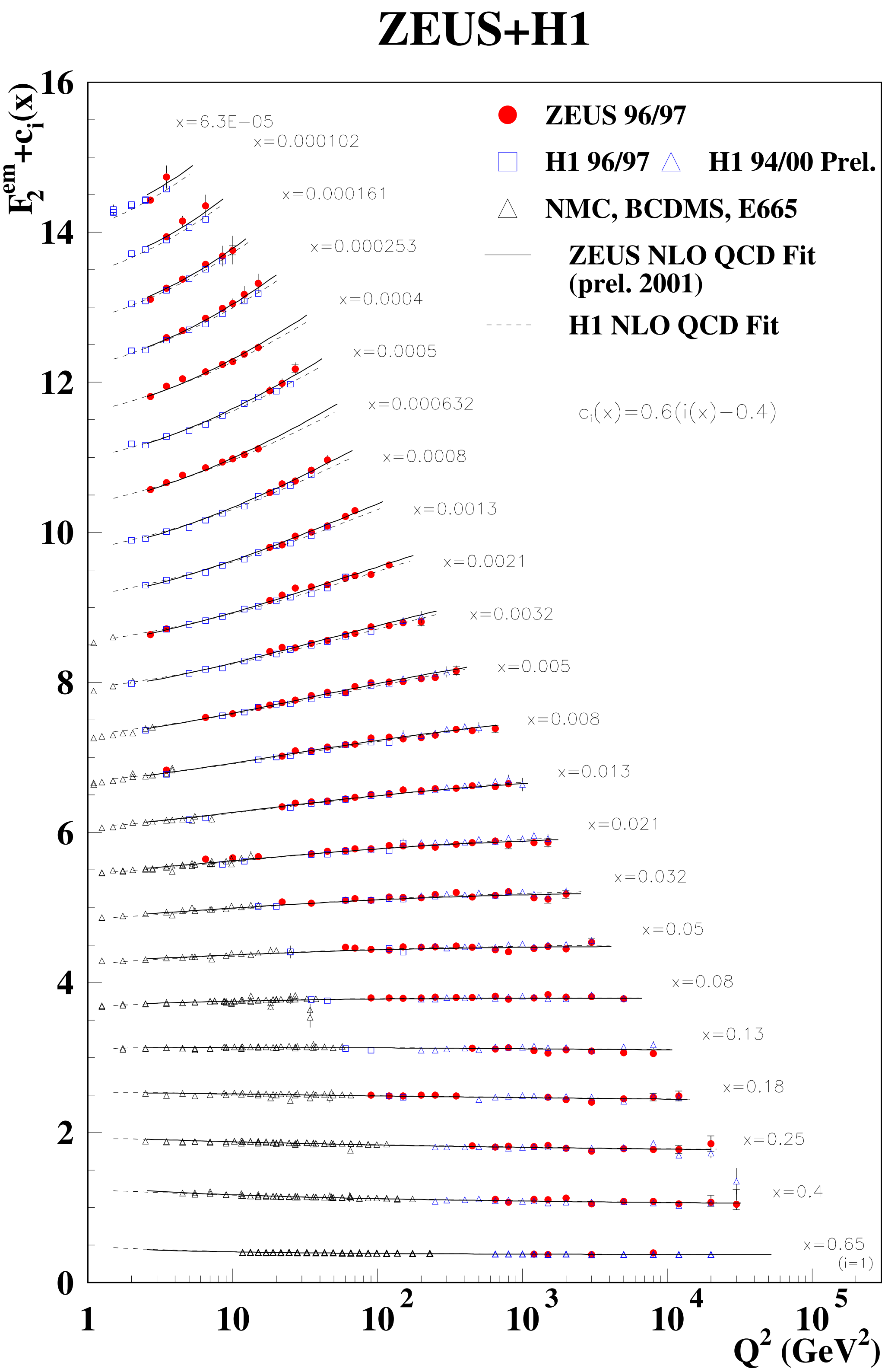

Figure 1: ZEUS and H1 values for F_2 versus Q^2 at different x, compared to the NLO fits. Here, each set of values for different x have been offset for clarity.

At sufficiently high E_T the relative contribution from final state long distance, non-perturbative effects such as hadronisation in studies of the final state is expected to be small and enable more meaningful comparison with next-to-leading (NLO) parton-level calculation, and in the case of events shapes, analytic models which might take account of these effects are now available in the form of power corrections [8].

2 NLO QCD fits to ZEUS and H1 data

Both HERA experiments ZEUS and H1 perform NLO fits to the F_2 structure function with α_S both constrained and as a free parameter in the fit. In order to constrain the fits in the kinematic region where the HERA data are not sensitive both collaborations also include additional data from fixed target experiments. In the case of ZEUS, additional data are used from the BCDMS [9], E665 [10] and NMC [11] collaborations, whereas H1 use only BCDMS data in addition.

The parametric form for the PDF's used by both collaborations is taken to be

$$f = p_1 x^{p_2}(1-x)^{p_3}(1+p_4\sqrt{x}+p_5 x). \quad (3)$$

In the case of ZEUS $p_4 = 0$ for all PDF's, while H1 take $p_4 \neq 0$ for the gluon distribution. Other significant differences in the fits are the treatment of heavy quarks – ZEUS uses the Roberts-Thorne variable flavour number (RT-VFN) scheme [12], whereas H1 use a fixed flavour number (FFN) scheme, and the treatment of systematic errors. However both collaborations fully take into account the point-to-point correlations [13].

The starting scale, Q_0, at which the PDF's are fixed is also different for each collaboration with ZEUS using $Q_0^2 = 7$ GeV^2 and H1 generally $Q_0^2 = 4$ GeV^2.

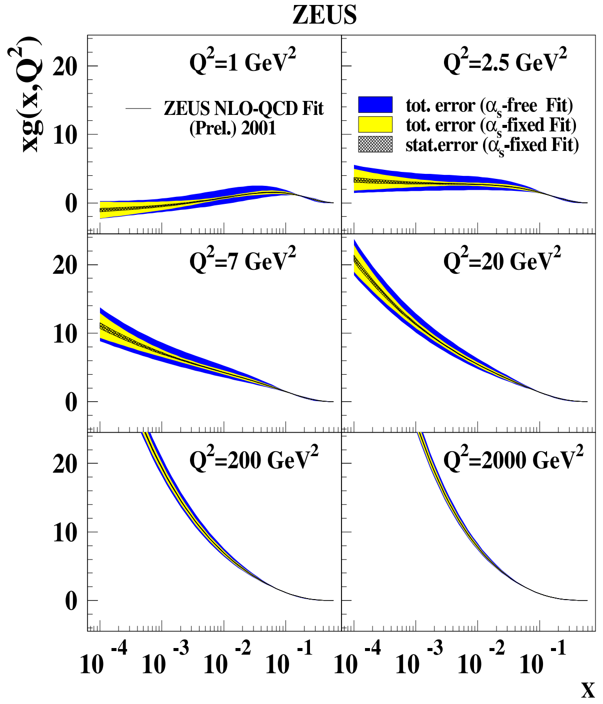

Figure 2: The extracted ZEUS gluon distribution.

Figure 1 shows both the ZEUS and H1 data on F_2 together with their respective fits. Typical of the data are statistical and systematic uncertainties of the order of 1% and 3% respectively. It is evident that the fits describe the data well over the entire kinematic plane for both the HERA and fixed target experiments, with the absolute fit uncertainty being largest at low x and Q^2.

Figure 3 shows the ZEUS F_2 data versus x compared to the NLO QCD fit, clearly illustrating the very steep rise towards low x, driven by the very steep gluon distribution. The gluon distribution extracted from the ZEUS fit is illustrated in figure 2. Fits with both α_S fixed, and as a free parameter are shown and illustrate the valance-like gluon distribution consistent with zero at low Q^2. The very steep rise of the gluon at low x is clearly seen, and it should be noted that the uncertainty improves with increasing Q^2,

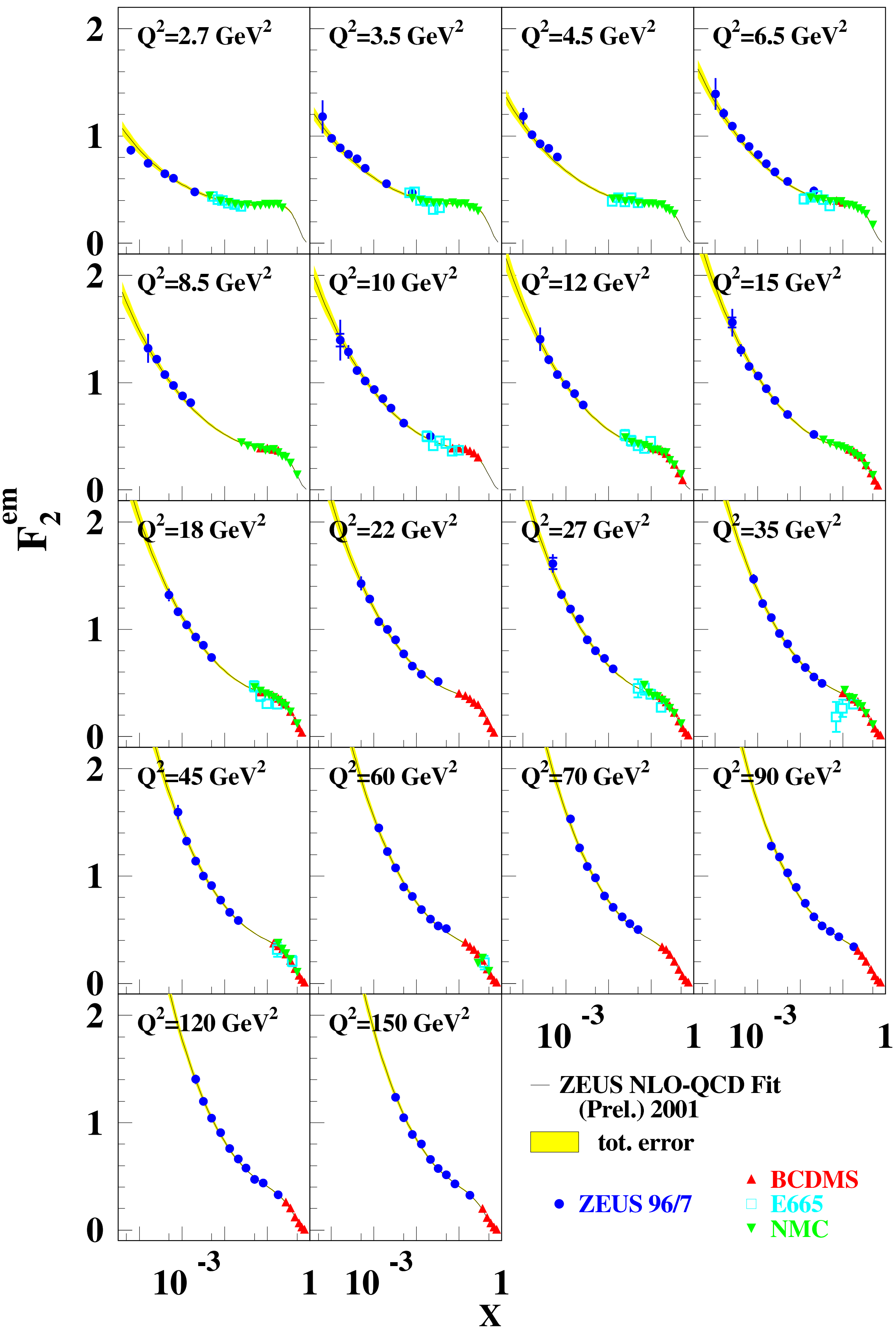

Figure 3: Comparison of the ZEUS F_2 width the NLO QCD fit versus x.

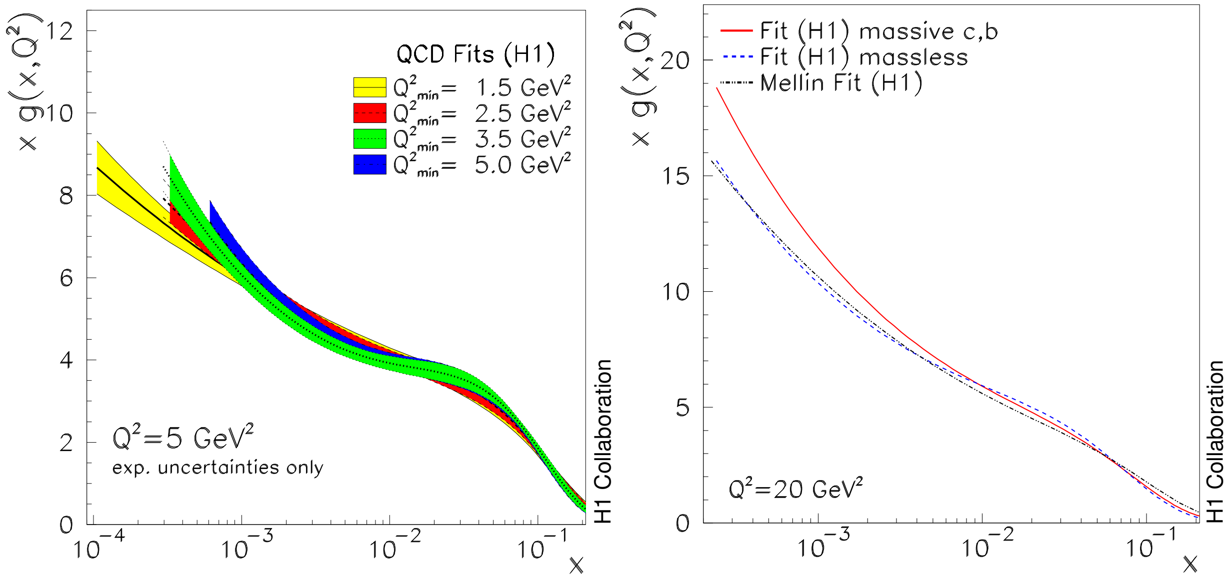

Figure 4: Dependence of the H1 fit on model assumptions.

such that for $10^{-3} < x < 10^{-1}$ the gluon distribution can be seen to be constrained to within $\sim 10\%$, with a small absolute, but large fractional uncertainty for $x > 0.1$ where the data are dominated by the valence quark distributions.

Figure 4 shows the dependence of the H1 fit on the model assumptions. The left figure illustrates the effect on the extracted gluon distribution of the choice of the minimum Q^2 of the data used in the fit, the inclusion of data at lower Q^2 clearly favouring a less steeply rising distribution. On the right, the effect of the choice of heavy quark treatment can be seen. Here the difference between the gluon distributions using either the FFN scheme, where the heavy flavours are produced purely dynamically via the boson gluon fusion (BGF) process and a zero mass variable number (ZM-VFN) scheme, where the heavy flavours are treated as massless partons above their production threshold, can be clearly seen, notably for $x < 10^{-2}$.

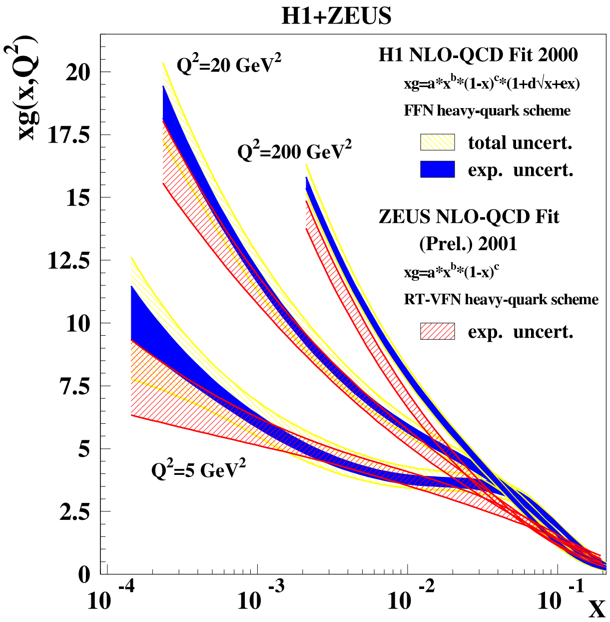

Figure 5: Comparison of the gluon distributions extracted by ZEUS and H1.

The H1 ZM-VFN scheme differs from the FFN scheme in that the ZM-VFN scheme is not expected to be particularly suitable at low Q^2 near the heavy flavour threshold, since mass effects are neglected, whereas the FFN scheme correctly includes mass effects but neglects large logarithms in Q^2/m_c^2 at high Q^2. In contrast, the RT-VFN scheme is a general mass VFN scheme which in some sense interpolates between the FFN

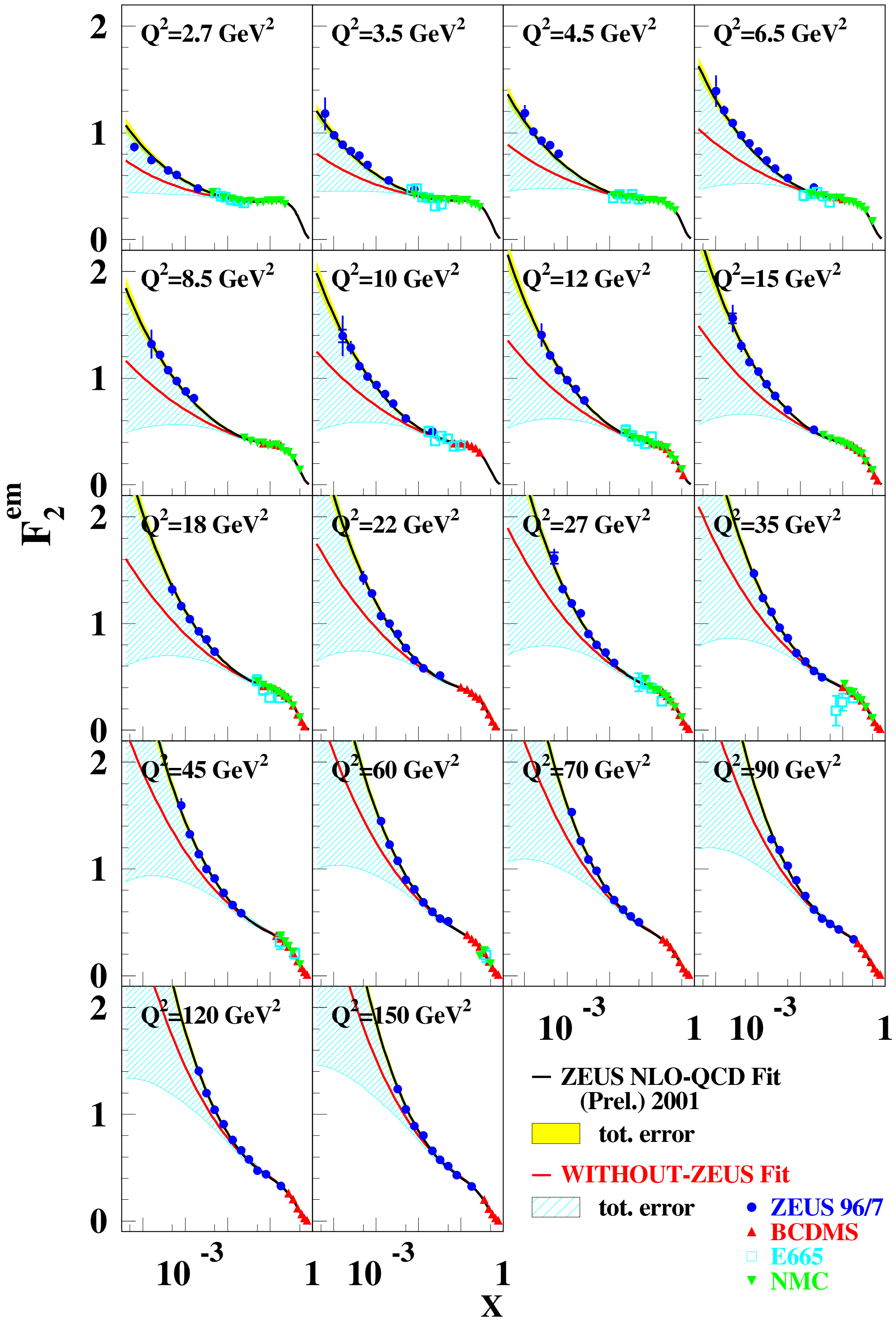

Figure 6: ZEUS F_2 data compared to a fit excluding ZEUS data.

scheme at low Q^2 and the ZM-VFM scheme at higher Q^2 and so is expected to be valid over a larger Q^2 range. However, the choice of heavy flavour treatment amounts to a scheme dependence of the unphysical PDF's rather than an uncertainty and so is not included in the model uncertainties.

A comparison of the gluon distributions extracted from the NLO fits of ZEUS and H1 at various Q^2 can be seen in figure 5. Although it appears that the H1 gluon distribution is predominantly higher than that extracted by ZEUS, they do appear broadly consistent. However, in order to make a more quantitative comparison, the differences arising from the different scheme dependences and model assumptions must be taken into account, notably the difference in the heavy flavour treatment and the different parametric form of the gluon PDF at high x arising from the $\sqrt{x}$ term. As yet, these issues are not fully resolved.

2.1 Impact of the HERA data

In order to study the impact of the HERA data on the results of the QCD fit, both H1 and ZEUS perform fits both including and excluding their choice of fixed target data.

Figure 6 shows the result of the ZEUS fit to F_2 data, but excluding the ZEUS data. From the figure, it is apparent that the HERA data lie only on the upper limit of the allowed fit, with the fixed target data preferring a significantly lower F_2. Until the advent of the HERA data, a flat distribution towards lower x could not be ruled out. For the fit excluding the HERA data, the uncertainty is seen to be very large since, in this case, the gluon distribution at lower x results only from the parametric form of the gluon fitted at higher x, where the contribution is smaller, and so is only weakly constrained.

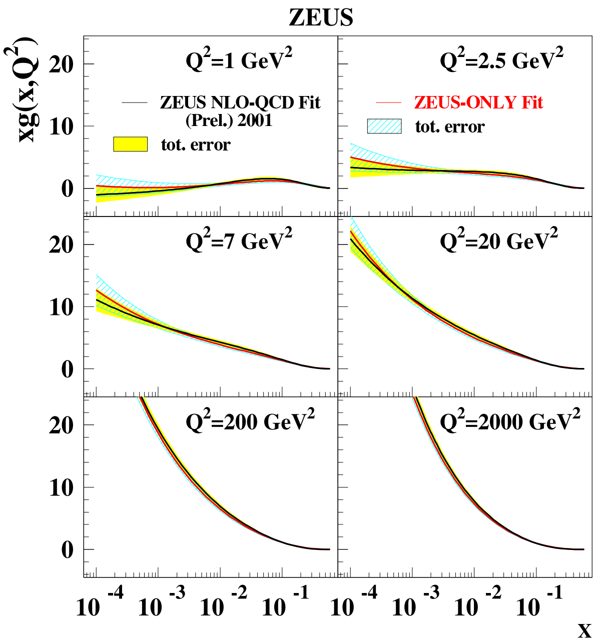

Figure 7: Extracted gluon distribution using a fit to ZEUS data alone.

Figure 7 in contrast, shows the resulting gluon distribution extracted from the fit to ZEUS data only. In this case, the form of the distribution is seen to be similar to that when including the fixed target data, but favouring a slightly steeper distribution than that with the fixed target data included. Again, this is due to the weak constraint on the gluon at large x, so the omission of the fixed target data has a small effect.

Since the gluon contribution to F_2 results predominantly from the BGF diagram, it is strongly correlated to the value for the coupling α_S. In order to extract a value for α_S fits were performed with α_S as a free parameter in the fit. The variation of the quality of the H1 fit as a function of the α_S value can be seen in figure 8. In this case, the resulting χ^2 distributions from fits to the H1 data, H1+BCDMS data and BCDMS data are shown.

For the case of the fit to the BCDMS data alone, the tendency for the fixed target data to prefer a lower gluon distribution results in a lower α_S value than obtained by the fits including the H1 data. However, here the inclusion of the fixed target data, while not greatly influencing the higher α_S value, do have the effect of improving the overall precision of the fit due to the constraint on the quark distributions at higher x.

The fit including both the H1 and BCDMS data, results in a value for the strong coupling, α_S, of

$$\alpha_S(M_Z^2) = 0.1150 \pm 0.0017(\text{exp.})^{+0.0009}_{-0.0005}(\text{model}) \pm 0.005(\text{scale}) \tag{4}$$

where the experimental uncertainty arises from statistical and correlated experimental systematic uncertainty and the model uncertainty is due to the choice of Q_{min}, the starting scale for the PDF's, heavy flavour masses, additional parameter choices and the use of additional terms in the parametric form of the PDF's. The scale uncertainty was estimated by varying the renormalisation and factorisation scales from $Q^2/4$ to $4Q^2$.

In the case of the ZEUS fit, the extracted value is found to be

$$\alpha_S(M_Z^2) = 0.1172 \pm 0.0008(\text{stat.}) \pm 0.0054(\text{syst.}) \tag{5}$$

where the first error results from the statistical and uncorrelated systematic experimental uncertainties, and the second from the correlated systematic uncertainties.

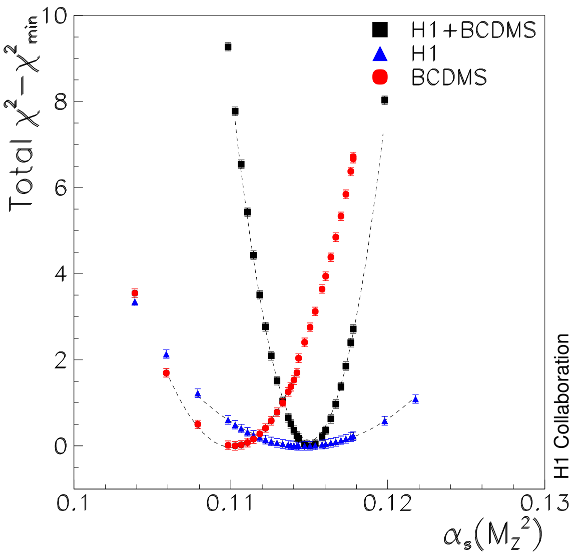

Figure 8: The variation of the fit quality for the H1 QCD fit as a function of α_S.

The scale uncertainty is now seen to be one of the dominant uncertainties on the precision of the extracted value of α_S from these fits, and suggests that the next-to-next-to-leading order (NNLO) corrections are still significant. The NNLO coefficient functions have been available for some time [14] and work current underway on calculating the NNLO splitting functions suggests that the resulting scale uncertainty will be greatly reduced [15].

3 Jet production in DIS

For the case of jet production in DIS, the cross-section can be factorised into a convolution of the PDF's in the target proton, f_a, with the hard sub-process cross-section, $\mathrm{d}\hat{\sigma}$,

$$d\sigma_{\text{jet}} = \sum_{a=q,\bar{q},g} \int \mathrm{d}x \; f_a(x, \mu_F^2) \; \mathrm{d}\hat{\sigma}_a(x, \alpha_S(\mu_R^2), \mu_R^2, \mu_F^2) \tag{6}$$

where μ_R and μ_F are the renormalisation and factorisation scales respectively. If the prediction including the detailed hard-subprocess provides a sufficiently consistent description of the data, then this in principle allows the extraction of α_S and the PDF's within the proton. Because of the strong correlation between the gluon distribution and α_S, typically when extracting α_S the PDF's are fixed from fits to inclusive DIS data with various fixed α_S values, such as the CTEQ4A [16] or MRST99 [17] series of PDF's.

The cross-section for inclusive single jet (1+1) production is not sensitive to the gluon distribution in the proton at it's leading order, whereas dijet (2+1) and higher multiplicity (n+1) jet production are directly sensitive to the gluon distribution, and hence α_S through the BGF subprocess.

In this case, jet production, where there are two natural large scales, Q and the jet E_T, raises the question of the choice of appropriate scale, in contrast to inclusive DIS with a single hard scale, Q. Therefore jet production in neutral current DIS enables the study of the QCD hard subprocess with a very high virtuality photon, providing complimentary, stringent tests of perturbative QCD.

3.1 Inclusive single jet and dijet production

Figure 9 shows the differential inclusive (1+1) jet production cross-section for jets measured with the K_T algorithm [18] measured by ZEUS. Here events are taken with at least one jet in the Breit frame [7] with transverse energy $E_T^{\text{Breit}} > 8$ GeV and with the jet psuedorapidity in the lab frame, $\eta_{\text{jet}}^{\text{lab}}$, in the range $-2 < \eta_{\text{jet}}^{\text{lab}} < 1.8$.

Also shown are the NLO predictions calculated using DISENT [19] using the scales $\mu_0 = Q$ and $\mu_0 = E_T^{\text{jet}}$, and including an estimation of hadronisation effects. Reasonable agreement with the data with a variation of the cross-section over five orders of magnitude can be seen. Also shown is the renormalisation scale uncertainty estimated using $\mu_0^2/4 < \mu^2 < 4\mu_0^2$. Using this data and the MRST99 series of proton PDF's [17], the strong coupling α_S has been extracted and results in

$$\alpha_S(M_Z^2) = 0.1190 \pm 0.0017(\text{stat.}) {}^{+0.0049}_{-0.0023}(\text{syst.}) \pm 0.0026(\text{th.}). \tag{7}$$

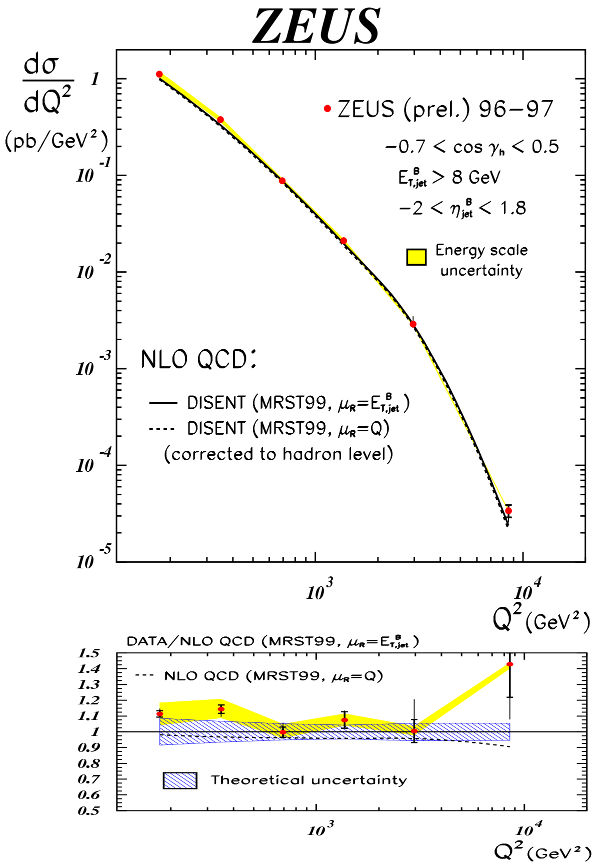

Figure 9: The inclusive jet cross-section as a function of Q^2 in NC DIS.

The largest source of theoretical uncertainty results from the variation of the renormalisation scale, although that from the PDF uncertainty is also reasonably large. The strong coupling extracted using inclusive 1+1 jet data measured by the H1 collaboration is discussed later and illustrated in figure 12.

Through the boson-gluon-fusion diagram, dijet (2+1) production in DIS is already, at leading order, sensitive to the gluon density in the proton and the strong coupling α_S.

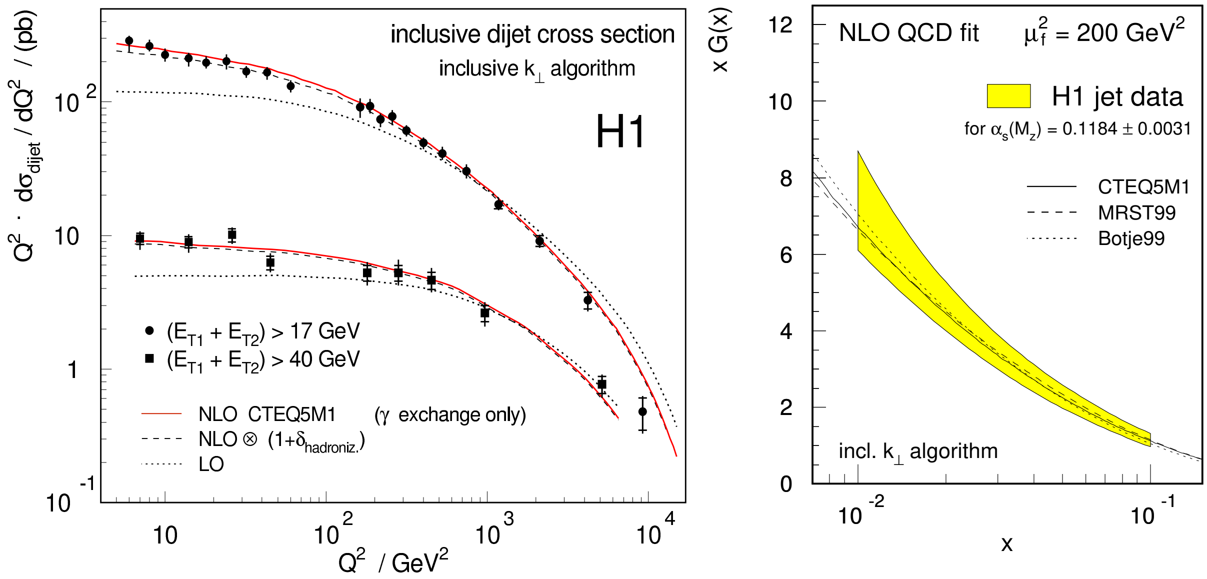

Figure 10: Comparison of the inclusive dijet production cross-section from H1 as a function of Q^2 with the predictions of NLO QCD (left) together with the extracted gluon distribution.

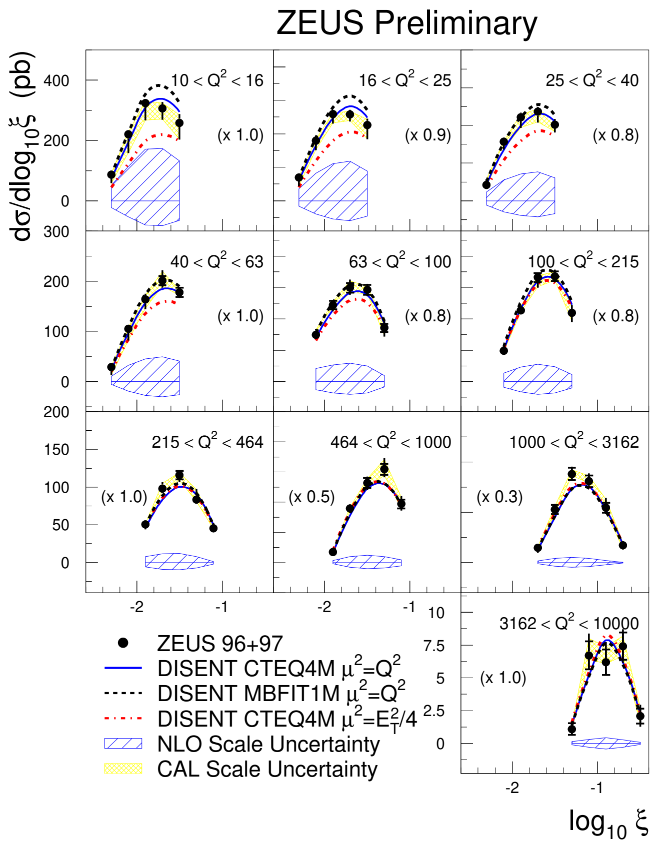

Figure 11: The differential dijet cross-section in DIS from ZEUS in bins of Q^2.

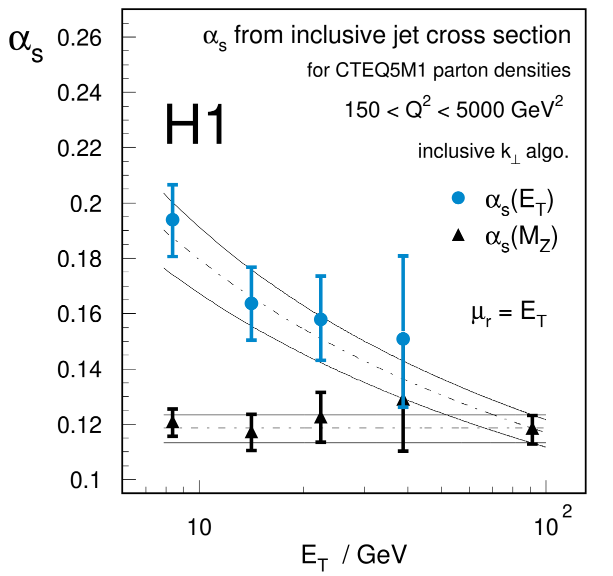

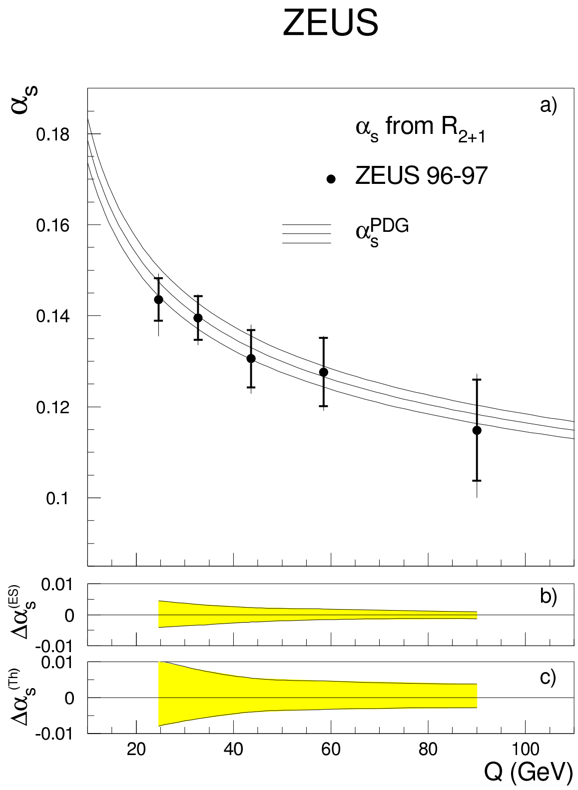

Figure 12: The running of α_S from ZEUS and H1 dijet data.

This makes it an interesting regime for the extraction of the gluon density within the proton. Figure 10 shows the dijet cross-section for jets measured with the K_T algorithm in the Breit frame with $E_T^{\mathrm{Breit}} > 5\mathrm{GeV}$ measured by H1. Again the NLO prediction shows reasonable agreement over the entire phase space, with the NLO corrections being significant at low Q^2.

Using the data on inclusive and dijet production, by fixing α_S, H1 have performed a fit using a fixed order NLO calculation to directly extract the gluon distribution in a complementary way to that from the global fits. The extracted distribution is illustrated in the right of figure 10 and is consistent with the central values from several other PDF sets, although the uncertainty is larger than that from fits to the inclusive data.

In a complementary analysis, ZEUS has also measured inclusive dijet production, as a function of the variable

$$\xi = x(1 + M_{\mathrm{jj}}^2/Q^2) \tag{8}$$

where M_{jj} is the invariant mass of the highest two jets in the event. For the case of dijet production at leading-order, ξ corresponds to the fraction of the proton momentum carried by the parton from the proton entering the hard sub-process. This cross-section is illustrated in bins of Q^2 in figure 11 compared to the results of the NLO prediction using two different PDF sets with the renormalisation scale uncertainty shown as the shaded band.

At high Q^2 where the scale uncertainty is smallest, the cross-section is dominated by the valence quark distributions and the difference between the PDF's cannot be distinguished. However, towards lower Q^2 the contribution from the BGF diagram becomes larger and the data become more sensitive to the gluon distribution in the proton. In this region differences between the predictions using the different PDF sets become apparent, indicating some discrimination between these sets. However in this regime the scale uncertainty also becomes larger, reaching the order of 50% for low Q^2. In addition, the difference in the predicted cross-section when using either Q or $E_T/2$ as the appropriate scale is large. In this region logarithms of Q^2/E_T^2 may be large so that at this low Q^2 unknown higher order corrections may still be significant.

Using the inclusive jet data and parton distribution functions from global fits to the inclusive DIS data, H1 has extracted the QCD coupling in five bins of E_T illustrated in the left of figure 12, clearly illustrating the running of α_s. Running the coupling back to the Z^0 mass, the following value is obtained

$$\alpha_s(M_Z^2) \quad = \quad 0.1181 \pm 0.0030(\mathrm{exp})^{+0.0039}_{-0.0046}(\mathrm{th})^{+0.0036}_{-0.0015}(\mathrm{pdf}), \tag{9}$$

when using the renormalisation scale $\mu_R = E_T$, and

$$\alpha_s(M_Z^2) \quad = \quad 0.1221 \pm 0.0034(\mathrm{exp})^{+0.0054}_{-0.0059}(\mathrm{th})^{+0.0033}_{-0.0016}(\mathrm{pdf}), \tag{10}$$

when using $\mu_R = Q$. It should be noted, that the precision of the extracted parameter is beginning to be comparable to the world average, and that the uncertainty is now dominated by that from renormalisation scale and PDF uncertainies from the theory.

In order to reduce the PDF uncertainty, ZEUS present two measurements of α_s using the cross-section for dijet production, and also the dijet rate – the ratio of the dijet cross-section to the inclusive cross-section. As in the case for the ZEUS measurement using inclusive 1+1 jet production, the error due to the uncertainties in the parton distributions is correctly estimated including their correlations by using the results of the MBFIT PDF's [20]. For the dijet rate the uncertainty due to the parton distribution functions, partially cancels to provide

$$\alpha_s(M_Z^2) = 0.1166 \pm 0.0019(\mathrm{stat})^{+0.0024}_{-0.0033}(\mathrm{syst})^{+0.0057}_{-0.0044}(\mathrm{th}). \tag{11}$$

where here, the PDF uncertainty is included in the theoretical uncertainty. In this case the dominant uncertainties arise from the renormalisation scale uncertainty, and the uncertainty on the ZEUS calorimeter energy scale.

3.2 Jet sub-structure

Besides the inclusive cross-section for jet production, the internal structure of the jets themselves can also provide information on the strong coupling through radiation from outgoing partons. This provides complementary information to that from jet production since it is less sensitive to the gluon distribution in the proton.

The lowest non-trivial contribution to jet sub-structure arises at $\mathcal{O}(\alpha_S)$ for single jet production. Using the integrated jet shape, $\Psi(r)$, defined as the fraction of the jet energy within a cone of radius, r, given by

$$\Psi(r) = \frac{1}{N_{\mathrm{jet}}} \sum_{\mathrm{jets}} \frac{E_T^{\mathrm{jet}}(r)}{E_T^{\mathrm{jet}}(R),} \tag{12}$$

ZEUS has extracted the strong coupling using jets in the range $21 < E_T < 55$GeV for $Q^2 > 125\mathrm{GeV}^2$ using fixed order NLO theory and the CTEQ4A series of PDF's.

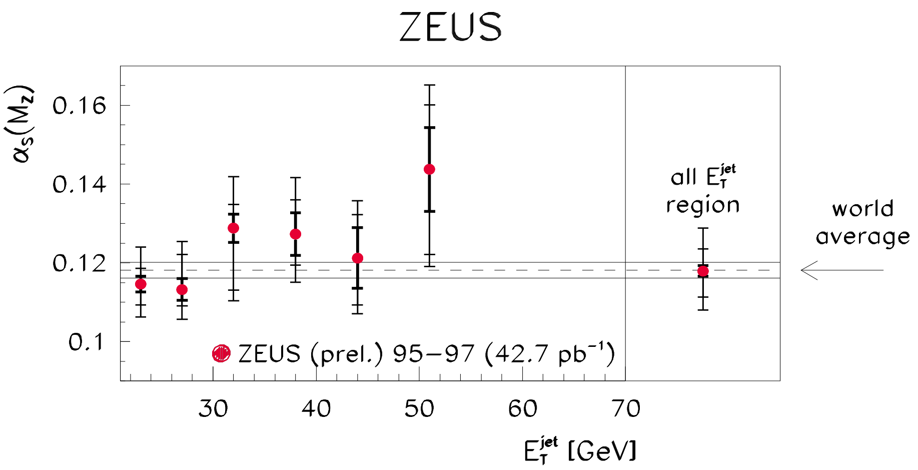

Figure 13: Extracted α_S values using ZEUS subjet multiplicity data

The results as a function of the jet E_T are illustrated in figure 13. Using the entire range of jet E_T an overall value of

$$\alpha_s(M_Z) = 0.1179 \pm 0.0014(\text{stat.})^{+0.0054}_{-0.0065}(\text{exp.})^{+0.0094}_{-0.0073}(\text{th.}) \tag{13}$$

is obtained, with a higher value of α_S being slightly favoured at higher E_T.

In addition ZEUS has also measured the strong coupling using the subjet multiplicity, where, the K_T algorithm is reapplied to the objects in each jet, until a distance parameter, d_{ij}, for all clustered objects, i and j fulfills

$$d_{ij} > d_{\text{cut}} = y_{\text{cut}}(E_T^{\text{jet}})^2.$$

Again using events with $Q^2 > 125\text{GeV}^2$, but this time with $E_T^{\text{lab}} > 15\text{GeV}$ the extracted strong coupling is measured to be

$$\alpha_S(M_Z^2) = 0.1185 \pm 0.0016(\text{stat.})^{+0.0067}_{-0.0048}(\text{syst.})^{+0.0089}_{-0.0071}(\text{th.}). \tag{14}$$

For both these measurements using jet substructure, as in the case of the extraction from the dijet rate, the largest uncertainty is that from the theory.

3.3 Three jet production

Besides the inclusive single jet and dijet data, the large data samples now collected be the ZEUS and H1 collaborations, make possible measurements of intrinsically higher order processes. Three jet production in DIS is an $\mathcal{O}({\alpha_S}^2)$ process at leading-order, and an NLO calculation has recently become available [21].

Figure 14 shows the H1 measurement of the three jet cross-section as a function of Q^2 together with the three-to-two jet rate, $R_{3/2}$, the ratio of the three-to-two jet cross-sections, enabling the the first comparison with theory of a subprocess in a hadronic collision calculated to $\mathcal{O}({\alpha_S}^3)$. Reasonable agreement is observed between the data and NLO calculation, with the three-to-two jet rate showing a reduced uncertainty from the

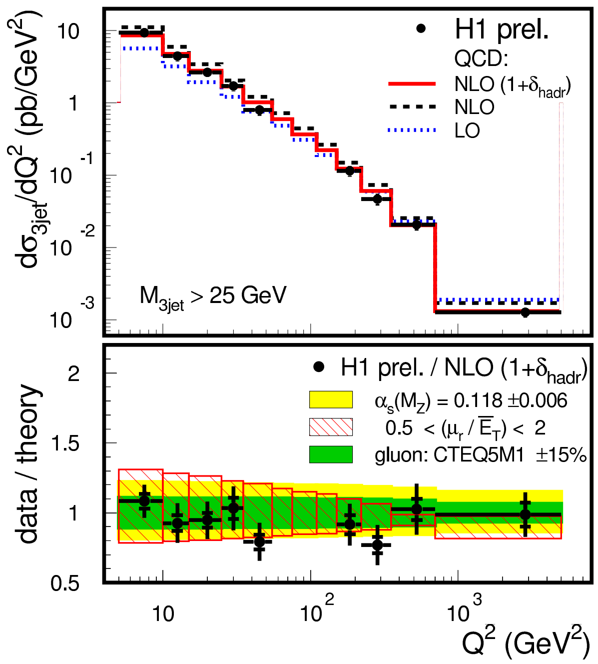

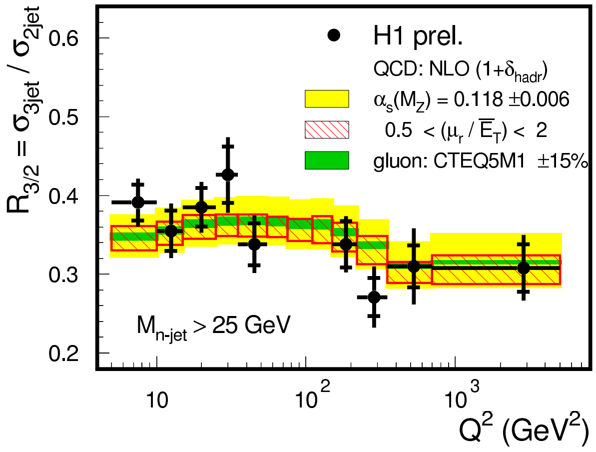

Figure 14: The inclusive three-jet production cross-section and 3-to-2 jet ratio in DIS measured by H1.

gluon in the proton. The smaller theoretical uncertainties mean that the future prospects for the extraction of α_S from this type of analysis are good, and should particularly benefit from the larger event samples expected with the upgraded HERA machine.

4 Summary of HERA α_S measurements

A summary of the α_S values extracted from the HERA data presented here can be seen in figure 15. Many complementary measurements of α_S using HERA data are now available, and all measurements are consistent with each other and the world average. For most of the measurements presented, the uncertainty is competitive with that from other sources, such as the LEP collaborations, and beginning to challenge the current world average. It will be interesting to see what impact the new HERA data will have on the world average.

In addition, it is informative to note, that with the new high precision data becoming available now, the dominant uncertainty in most cases arises from the theory – especially the renormalisation scale uncertainty. It will be interesting to see what implications the calculation of the NNLO cross-section will have for this uncertainty.

5 Event shapes in DIS

Besides jet production, studies of event shape variables in DIS also yield valuable information on the QCD hard sub-process and the QCD coupling constant. Recently, power correction models have become available [8] which in some sense provide an analytic framework for the transition of partons to hadrons by integrating over the strong coupling at small scales. These introduce a single, additional non-perturbative parameter which represents the effective strong coupling below the cutoff for pQCD calculations.

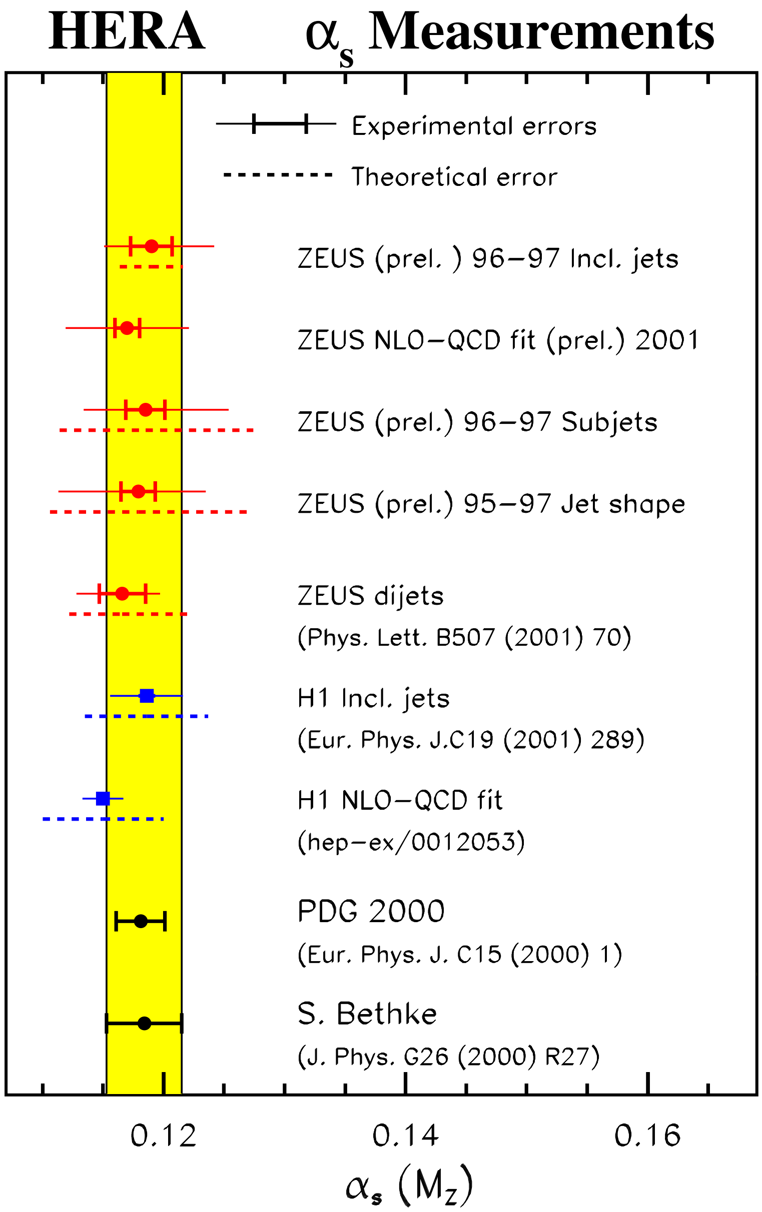

Figure 15: A summary of α_S values from HERA compared to the world average.

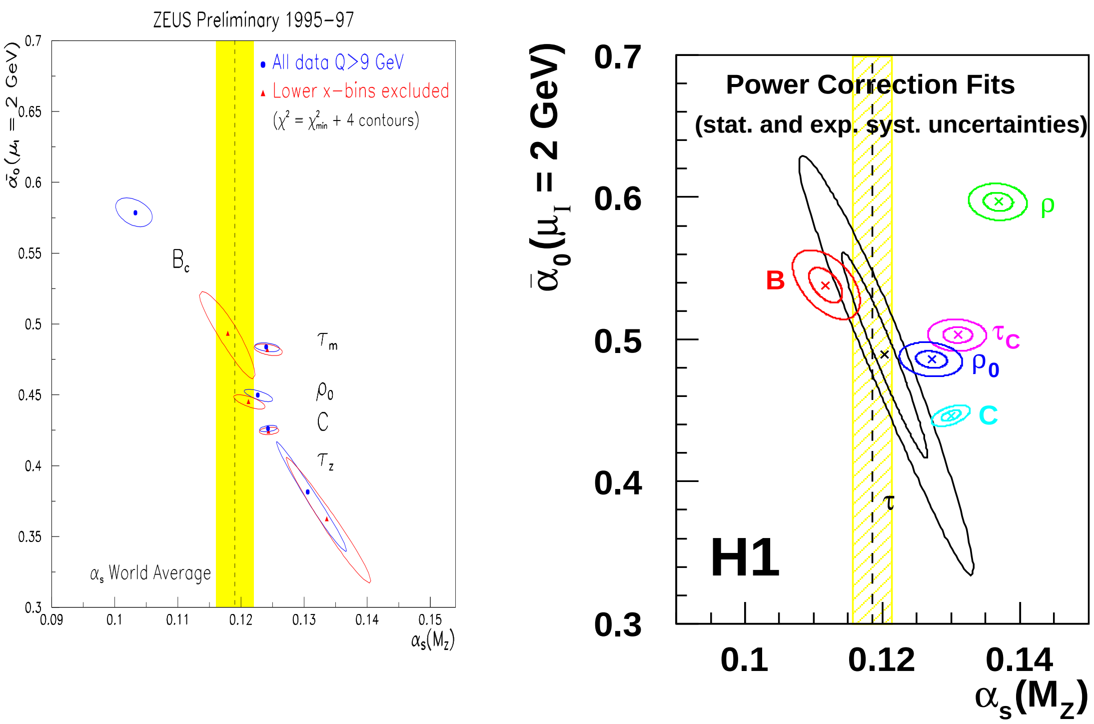

Figure 16: Values for α_S and $\bar{\alpha}_0$ fitted to the mean event shapes in the Breit frame from ZEUS and H1.

This parameter must be experimentally determined and is expected to be universal. By studying event shapes in the current fragmentation region of the Breit frame in DIS comparison can be made with results from e^+e^- annihilation and so test the universality of these models.

For a general event shape F, the mean value can be decomposed into a perturbative component and a term due to the power correction model

$$< F >=< F >^{\rm pert} + < F >^{\rm pow} \tag{15}$$

where $< F >^{\rm pow}$ is of the form $1/Q^p$.

The power correction is then characterised by a non-perturbative parameter, $\bar{\alpha}_{p-1}(\mu^2)$, and by fitting a power correction with $p = 1$, of the form

$$< F >^{\rm pow}= a_F \frac{32\mathcal{M}}{3\pi^2 p}\left\{\frac{\mu_I}{Q}\right\}^p \left[\bar{\alpha}_{p-1}(\mu^2) - \alpha_s(Q^2) - \frac{\beta_0}{2\pi}\alpha_s^2(Q^2)\left\{\ln\frac{Q}{\mu_I} + \frac{K}{\beta_0} + \frac{1}{p}\right\}\right] \tag{16}$$

simultaneously for $\bar{\alpha}_0(\mu^2)$ and $\alpha_s(\mu^2)$ the strong coupling can be extracted.

Both ZEUS and H1 have measured the mean values of several event shapes variables, for example, the *thrust* (τ), *jet broadening* (B), and *jet mass* (ρ). The values of α_S and $\bar{\alpha}_0$ from the resulting fits to the mean event shapes as a function of Q^2, excluding the low Q^2 region, as measured by H1 and ZEUS are shown in figure 16. Here, the data are seen to cluster around α_S values reasonable near the world average, but the spread in $\bar{\alpha}_0$ is reasonably large. ZEUS measure the mean event shapes as a function of x and notably for the jet broadening and thrust, observe a clear x dependence, not present in the power correction model.

As such, the obtained values are considered to be reasonably consistent with a single value of $\bar{\alpha}_0(\mu^2)$ given that the theoretical uncertainties (not shown) are large. In addition the obtained values for α_S are reasonably widely spread suggesting that in the DIS regime, higher order effects may still be significant.

6 Conclusions

HERA has now produced a wealth of precision inclusive and high E_T jet data in DIS, where the running of α_S can be studied over many orders of magnitude within a single environment. Fits to the inclusive HERA data now provide the coupling, α_S, with a mean value and precision compatible with the world average.

Fits to jet data assuming the parton density functions of the proton from inclusive data provide many consistent measurements of α_S and challenge the precision of the current world average – the dominant uncertainty often resulting from theory.

The gluon distribution from HERA inclusive and jet data are in reasonable agreement given the different assumptions, with the resulting gluon distributions seen to rise significantly more steeply at low x than previously suggested by fixed target data. From the NLO-QCD fits, the HERA data alone are seen to constrain the proton gluon distribution to within 10% at intermediate to high Q^2 and $10^{-4} < x < 10^{-1}$.

Both the HERA inclusive and jet data in DIS are described well by NLO-QCD for up to five orders of magnitude in Q^2 and four orders of magnitude in x which can be seen as a major triumph of perturbative QCD.

Following the HERA luminosity upgrade high precision data at the highest Q^2 will become available enabling even more stringent constraints to be placed on the QCD coupling and the parton distributions within the proton.

7 Acknowledgements

The author would like to thank the QFTHEP Organising Committee for a very enjoyable conference and a very pleasant stay in Moscow.

References

[1] ZEUS Collaboration; Phys.Lett. **B345** (1995) 576;
H1 Collaboration; Phys.Lett. **B354** (1995) 494

[2] ZEUS Collaboration; Eur.Phys.J. **C21** (2001) 443
H1 Collaboration; Eur.Phys.J. **C21** (2001) 33

[3] ZEUS Collaboration; Phys. Lett. **B507** (2001) 70;
H1 Collaboration; Eur. Phys. J. **C19** (2001) 289

[4] V.N.Gribov and L.N.Lipatov; Sov J. Nucl. Phys **15** (1972) 438;
L.N.Lipatov; Sov J. Nucl. Phys **20** (1975) 94;
Yu.L.Dokshitzer; Sov. Phys. JETP **46** (1977) 641;
G.Altarelli and G.Parisi; Nucl. Phys. **B126** (1977) 298

[5] L.N.Lipatov; Sov. J. Nucl. Phys. **23**(3) (1976) 338
Ya.Ya.Balitskii and L.N.Lipatov; Sov. J. Nucl. Phys. **28**(6) (1978) 822
E.A.Kuraev, L.N.Lipatov and V.S.Fadin; Sov. Phys. JETP **45**(2) (1977) 199

[6] J.Cole; These proceedings.

[7] R.P.Feyman; Photon-hadron interactions, Benjamin NY (1972).

[8] Yu.L.Dokshitzer and B.R.Webber; Phys. Lett. **B352** (1995) 451; ibid. **B404** (1997) 321;
Yu.L.Dokshitzer, G.Marchesini and G.P.Salam; Eur. Phys. J. (direct) **C3** (1999) 1, *and Erratum*: ibid. **C1** (2001) 1

[9] BCDMS Collaboration; Phys. Lett. **B223** (1989) 485; ibid. **B237** (1990) 592

[10] E665 Collaboration; Phys. Rev. **D54** (1996) 3006

[11] NMC Collaboration; Nucl. Phys. **B483** (1997) 3; ibid. **B487** (1997) 3

[12] R.G.Roberts, R.S.Thorne; Phys. Lett. **B421** (1998) 303

[13] C.Pascaud and F.Zomer; LAL 95-06

[14] W.L.van Neerven and E.B.Zijlstra; Phys. Lett. **B272** (1991) 121; ibid. **B273** (1991) 476; ibid. **297** (1992) 377; Nucl. Phys. **B383** (1992) 525.

[15] W.L.van Neerven and A.Vogt; hep-ph/0006154 (2000)

[16] H.L.Lai *et al*; Phys. Rev. **D55** (1997) 1280

[17] A.D.Martin *et al*; Eur. Phys. J **C4** (1998) 463 Eur. Phys. J **C14** (2000) 133

[18] S.Catani *et al.* Phys.Lett. **B285** (1992) 291

[19] S.Catani and M.H.Seymour; Nucl. Phys. **B485** (1997) 291, *and Erratum* **B510** (1997) 503.

[20] M.Botje; Eur.Phys.J. **C14** (2000) 285

[21] Z.Nagy and Z.Trócsányi; Phys. Rev. Lett. **87** (2001) 082001